SF2A 2022
J. Richard, A. Siebert, E. Lagadec, N. Lagarde, O. Venot, J. Malzac, J.-B. Marquette, M. N'Diaye, D. Briot (eds)

PROBING THE CENTRAL ENGINE OF CORE-COLLAPSE SUPERNOVAE WITH THEIR MULTI-MESSENGER EMISSION

M. Bugli[1], J. Guilet[1], T. Foglizzo[1] and M. Obergaulinger[2]

Abstract. The multi-messenger emission produced by core-collapse supernovae provides a unique way to probe the first seconds of the stellar explosion and directly measure the properties of the still-forming hot proto-neutron star. We will review the main properties of the gravitational waves (GW) emitted during core-collapse supernova explosions, linking them to the dynamical evolution of the central engine. We will then present recent results of 3D numerical models that take into account fast rotation and strong magnetic fields, showing the impact of the magneto-rotational explosion mechanism on the GW and neutrino emission.

Keywords: core-collapse supernovae, gravitational waves, neutrinos, multi-messenger, instabilities, magnetic fields

1 Introduction

Core-collapse supernovae (CCSN) represent an extraordinary laboratory to understand how stellar-mass compact objects form and how the Universe is enriched by the heavy elements they disseminate after the explosion. The gravitational collapse of a massive star at the end of its life leads to a huge increase in its central density, and as matter de-leptonizes, a continuous flux of neutrinos starts being emitted from the central region of the star. Densities reach nuclear values of $\rho \sim 10^{14}$ g/cm^3 within a few hundred milliseconds, at which point the in-falling material bounces over the dense core, forming a shock wave that starts propagating outwards. As the shock reaches lower densities, a burst of electron neutrinos ν_e (previously trapped in the dense core) is suddenly emitted, while neutrinos and anti-neutrinos of all flavors are emitted from the central hot proto-neutron star (PNS). The ram pressure of the collapsing stellar layers and the continuous energy losses due to the dissociation of iron-group elements crossing the shock wave lead to a stalling phase, during which the shock stops its expansion and fails to propagate further. The physical process responsible for the revival of the shock in the vast majority of CCSN is the so-called *neutrino heating mechanism*: a fraction of the neutrinos emitted from the PNS are absorbed by the shocked matter, depositing their energy and pushing the shock front towards the surface of the stellar progenitor.

The initial gravitational binding energy (typically $\sim 10^{53}$ erg) is almost entirely radiated away during the gravitational collapse in the form of neutrinos ($\sim$99%), while the remaining fraction is used to launch the ejecta during the stellar explosion. A very small part of the energetic budget ($\sim 10^{-8}$) is also emitted in the form of gravitational waves, which are produced by fluid instabilities and oscillations occurring within the highly dense PNS. The emission of gravitational waves and neutrinos during the early stages of the collapse and the shock's propagation provides a unique window on the dynamics of the forming proto-neutron star, which cannot be directly probed by observing electromagnetic radiation. In the present work we briefly review the general features of GW emission expected from core-collapse supernovae and computed via multi-dimensional numerical models. We will focus then on the effects of rotation, and in particular on the signatures left by non-axisymmetric large-scale fluid instabilities within the PNS (Bugli et al. 2022). Lastly, we will present results from recent 3d MHD models (Bugli et al. 2021) that display the effect of strong magnetic fields on the CCSN multi-messenger emission (Bugli et al. 2022).

[1] Université Paris-Saclay, Université Paris Cité, CEA, CNRS, AIM, 91191, Gif-sur-Yvette, France
[2] Departament d'Astronomia i Astrofísica, Universitat de València, Dr. Moliner 50, 46100, Burjassot, Spain

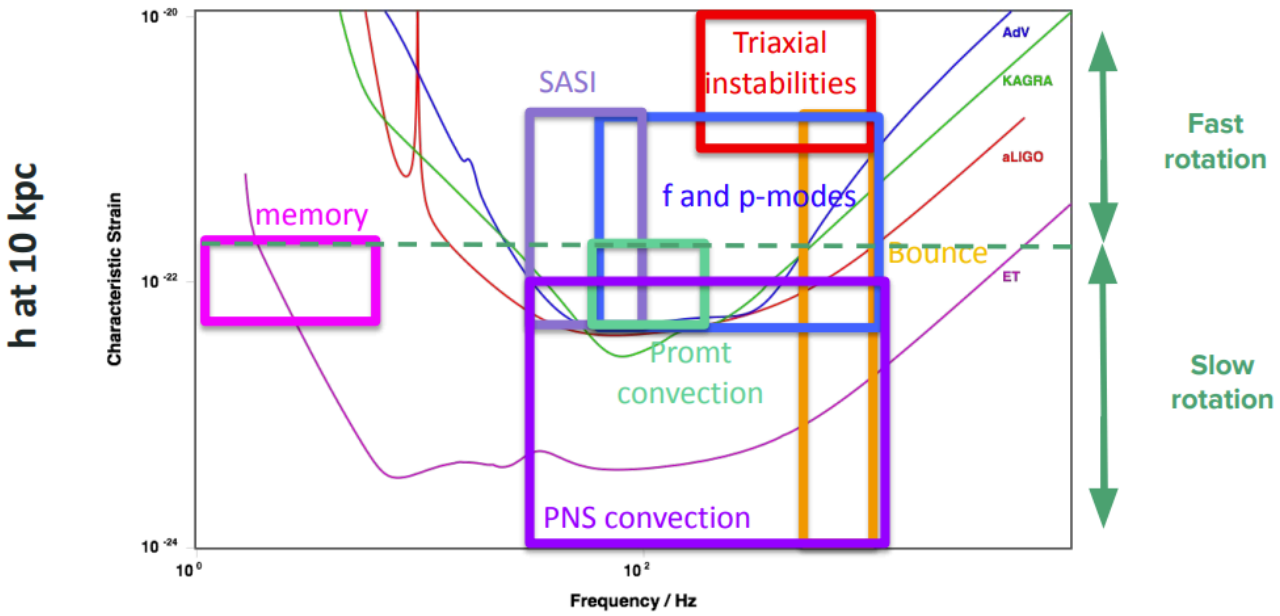

Fig. 1. Main contributions to the GW signal produced by core-collapse supernovae (credit: Pablo Cerdà-Duràn).

2 GW signals from standard CCSN

The GW emission of CCSN is fundamentally related to the onset of dynamical perturbations in the central PNS, which is the only region of the collapsing stellar progenitor dense enough to produce a detectable signal. The main contributions to the signal are summarized in Fig. 1.

2.1 Primary features

One of the most important signatures in the GW emission of standard non-rotating CCSN is induced by oscillating modes in the PNS, which can be excited mainly by two physical processes: 1) the convection within the PNS driven by the lepton gradient; 2) the activity of the *Standing Accretion Shock Instability* (SASI) interacting with the PNS. The former mechanisms leads to the emergence of f and $p-$modes whose oscillation frequency increases steadily with time from ~ 100 Hz up to ~ 1 kHz, as a consequence to the steady compression of the PNS during the ongoing gravitational collapse. By identifying the modes signature it is possible to establish universal relations that provide a parametric description of the frequency evolution in terms of the PNS mass and radius (Torres-Forn et al. 2019). Such relations are extremely important, as they allow us to recover constraints on the PNS properties directly from the gravitational signal. The direct signature of SASI, instead, is typically at lower frequencies ($\lesssim 100$ Hz) and does not increase with time, as the increase in pressure of the PNS has little effect on the typical time-scale of the shock instability (Andresen et al. 2017; Kawahara et al. 2018).

2.2 Secondary features

There are other physical processes that can modulate the GW emission from non-rotating CCSN. For instance, the *prompt convection* triggered by the initial shock expansion and neutrino outburst produces a short-lived signal (~ 100 ms) at a frequency of 50-100 Hz (Murphy et al. 2009). A persistent non-sphericity of the shock front can also produce a low frequency modulation of the emission ($\sim 1-10$ Hz), which could be marginally detected only by the next generation of ground-based observatories (Murphy et al. 2009). Finally, the long-term convection in the PNS driven by the lepton gradient can sustain a weaker GW signal in the 100-1000 Hz range that can last up to ~ 50 s (Raynaud et al. 2021).

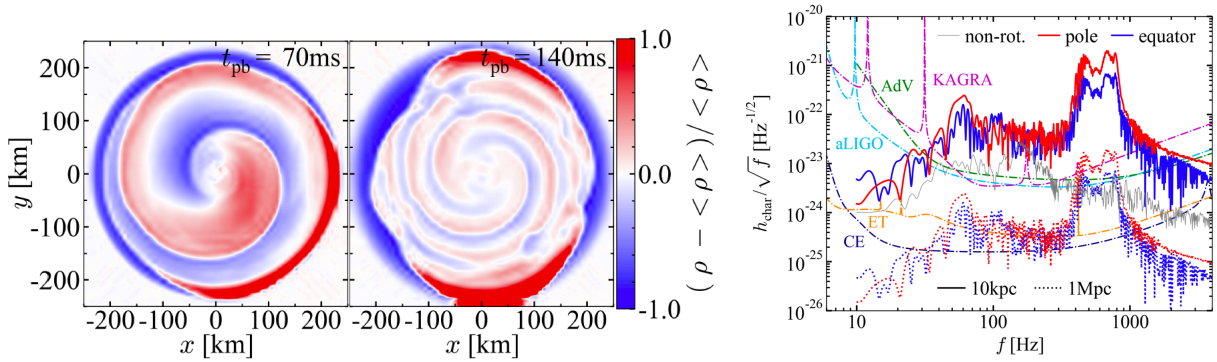

Fig. 2. Left: Non-axisymmetric density deviations on the equatorial plane during the development of the low $T\|W|$ instability (from Shibagaki et al. (2020)). **Right:** Characteristic GW spectral amplitudes for the same model depicted on the left panel (from Shibagaki et al. (2020)).

2.3 The impact of rotation

The inclusion of rotation has important consequences for the overall explosion dynamics and the evolution of the PNS (Takiwaki et al. 2016; Summa et al. 2018), which has important consequences for the GW emission. The first signature of rotation on the multi-messenger emission comes at bounce, when the axisymmetric oscillations in the quadrupolar moment induced in the PNS by rotation produce a distinctive burst followed by a ring-down (Ott 2009). Such signal has a frequency of typically a few hundred Hz, and its production is favored in case of moderate to fast rotation (i.e. for angular velocities of $\Omega \sim 1 - 10$ rad/s).

Fast rotation has another important effect on the PNS dynamics, which is triggering the growth of the so-called *low* $T/|W|$ *instability* (Passamonti & Andersson 2015; Takiwaki et al. 2021). The onset of such instability leads to the formation of large-scale non-axisymmetric perturbation in the PNS, with typical azimuthal number $m = 1, 2$ (left panel of Fig. 2), which produce a strong and persistent GW emission (Shibagaki et al. 2020). Such signal has an initial frequency of a few hundred Hz, which increases stadily due to the ongoing compression of the PNS and can reach values of the order of ∼kHz. Numerical models have shown that the GW signal due to the low $T/|W|$ instability has the highest amplitude w.r.t. the other components presented so far, and could indeed by detected by the current generation of ground-based GW observatories for a galactic event at a distance of 10 kpc (right panel of Fig. 2).

3 GW signals from magnetized CCSN

While the neutrino-heating mechanism provides a solid scenario for the explosion of standard CCSN producing ejecta energy of $\sim 10^{43}$ erg, it is more difficult to use it to explain the onset of outstanding stellar explosions such as hypernovae (Drout et al. 2011) and super-luminous supernovae (Nicholl et al. 2013). To account for the extra energy required to power up these transients, a combination of fast rotation and strong magnetic fields is often invoked, with the former providing the energy reservoir and the latter the means to extract it efficiently. Numerical simulations of magneto-rotational explosions have become in the past two decades more accessible than ever, with numerous different research group producing MHD CCSN simulations that show strong bipolar outflows during the explosion (Shibata et al. 2006; Burrows et al. 2007; Takiwaki et al. 2009; Obergaulinger & á. Aloy 2017; Kuroda et al. 2020; Bugli et al. 2020; Obergaulinger & Aloy 2021; Bugli et al. 2021). Besides affecting the shock dynamics, magnetic field with strong rotation can also lead to efficient dynamo action within the PNS (Raynaud et al. 2020; Reboul-Salze et al. 2021, 2022; Guilet et al. 2022), which in the case of magnetic convection can even leave a characteristic signal in the GW emission (Raynaud et al. 2021).

In Bugli et al. (2021) we presented a series of 3d CCSN simulations which considered the massive stellar progenitor 35OC (Woosley & Heger 2006) with its original fast rotation profile, but superimposing different magnetic fields. Since the fields amplified by the PNS dynamos generally have a complex topology, the magnetic fields included in the models are an aligned dipole, equatorial dipole, and an aligned quadrupole. We also reproduced a hydrodynamic benchmark, which provides the means to assess the importance of the dynamic role of magnetic fields in the core-collapse evolution and the related multi-messenger emission.

In the top panels of Fig. 3 we report the spectrogram of the GW characteristic strain $h_{\rm char}$ observed along

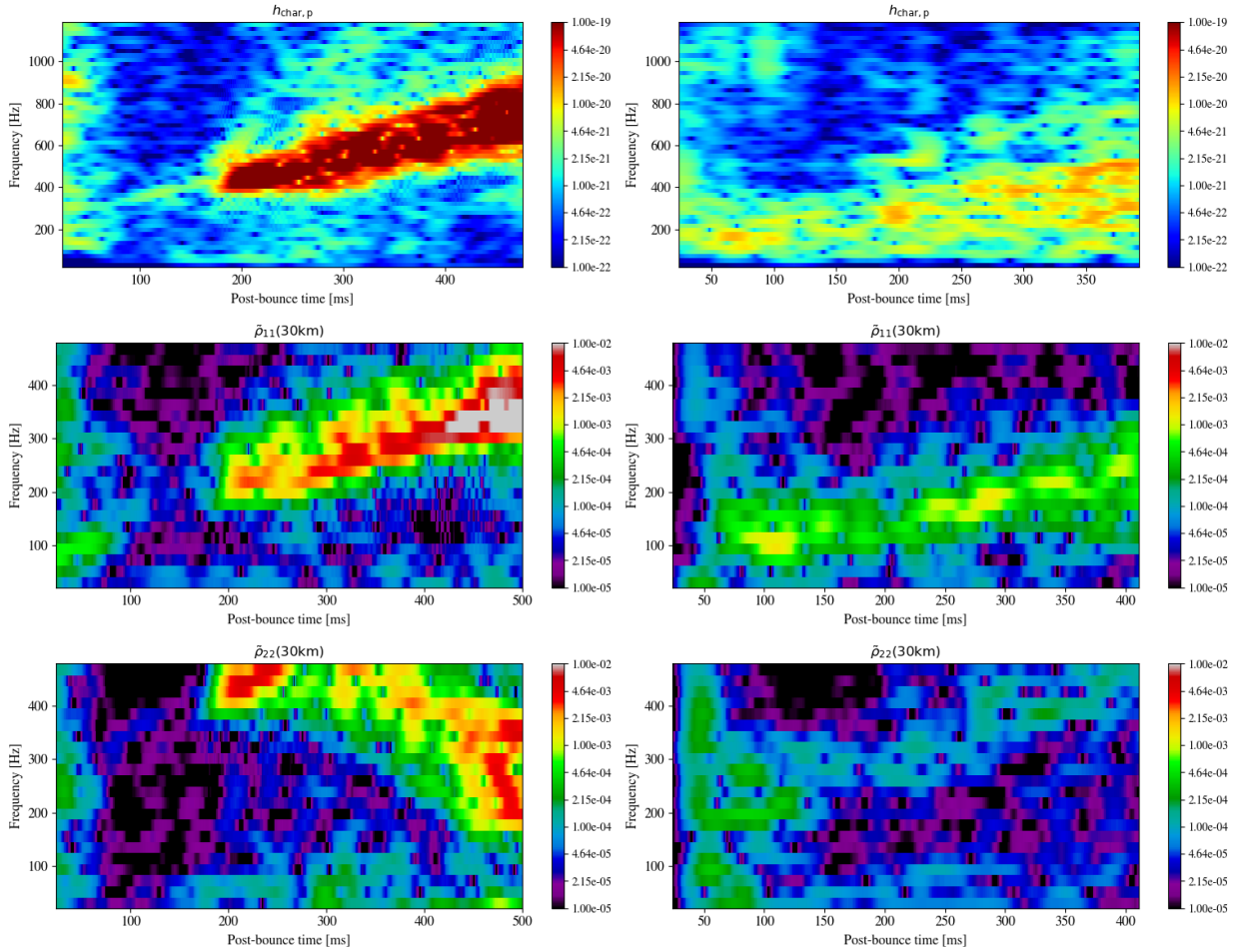

Fig. 3. Top: Time-frequency diagrams of the characteristic GW strain assuming a distance of 10 kpc for the hydrodynamic model (left) and the magnetized model with an aligned dipole (right). **Middle:** Time-frequency diagrams of the $(l = 1, m = 1)$ mode in the density distribution within the PNS at $r = 30$ km for a hydrodynamic model (left) and the magnetized model with an aligned dipole (right). **Bottom:** same as the middle panels, but for the $(l = 2, m = 2)$ mode.

the rotational axis of the model for an event at a distance of $D = 10$ kpc. The left panel, which refers to the hydrodynamic benchmark, presents a strong emission starting at $t \sim 200$ ms, which starts at a frequency of 400 Hz that steadily increases. We can identify the source of the emission as the action of the low $T/|W|$ instability, as it corresponds to the emergence of large-scale non-axisymmetric modes in the PNS (middle and bottom left panels of Fig. 3). The frequency of the $l, m = 1, 1$ mode is half of the one observed in the GW signal, while that of the $l, m = 2, 2$ mode matches well the pattern in GW up to $t \sim 350$ ms p.b., after which the signal is aliased to frequencies below 500 Hz (due to the limited sampling rate of 1 kHz for the simulation's output). The aliasing effect is instead absent in the GW signal, as it is sampled at a frequency 10 times higher.

On the other hand, the model with an aligned dipolar field produces a GW signal which is an order of magnitude weaker, with a broader spectral shape and a generally lower frequency (right panel of Fig. 3). At the same time, the large-scale oscillation mode in the PNS are also much weaker w.r.t. the hydrodynamic case (middle and bottom right panels), with the $l, m = 2, 2$ mode being much weaker than the $l, m = 1, 1$ one. Such drastically different behavior is due to the very efficient transport of angular momentum induced by the large-scale magnetic fields, which flattens the rotational profile through the PNS and stabilizes against the low $T/|W|$ instability (Bugli et al. 2022). This explains also the lower frequency of the signal, since the magnetorotational mechanism significantly slows down the PNS.

A qualitatively similar scenario is presented by the other magnetized models, despite the different radial profiles of the angular velocity. This suggests that as long as angular momentum is extracted from the PNS and rotation tends towards the solid-body case, the PNS dynamics connected to the emission of GW is rather

similar.

4 Neutrinos

Finally, we briefly analyze some properties of the neutrino signal produced by the numerical models presented so far. Strong magnetic fields have also an important role in modulating the emission of neutrinos. This can be evinced from the left panel of Fig. 4, where we report the lightcurve of the electron neutrino luminosity L_{ν_e} measured along the equatorial line-of-sight at 500 km from the center. The hydrodynamic model produces systematically a higher luminosity w.r.t. the magnetized models, which display very similar values of L_{ν_e} among themselves. This dichotomy is a consequence of the more oblate shape of the PNS in presence of strong magnetic fields, as the outward transport of angular momentum leads to stronger rotational support at the equator and hence larger neutrinospheres. As a direct consequence, the neutrinos emitted along the equatorial plane are less energetic (being produced at lower temperatures) and their associated luminosity is weaker (Bugli et al. 2020, 2022).

If we decompose the neutrino lightcurves in a time-frequency diagram (right panels of Fig. 4) we can see that in the hydrodynamic case there are clear features resembling the PNS oscillation modes depicted in Fig. 3. There are also excesses of signal at low frequencies which are induced by the non-axisymmetric SASI modes (Shibagaki et al. 2021). On the other hand, the model with an aligned dipole shows neither clear features connected to the azimuthal large-scale modes in the PNS or low frequency bursts, since it produces a prompt magneto-rotational explosion and does not develop SASI to a significant extent. A similar behaviour is reproduced by the other magnetized models, with the exception of some low-frequency SASI-related features which can develop when the magneto-rotational mechanism is less efficient (Bugli et al. 2020, 2021).

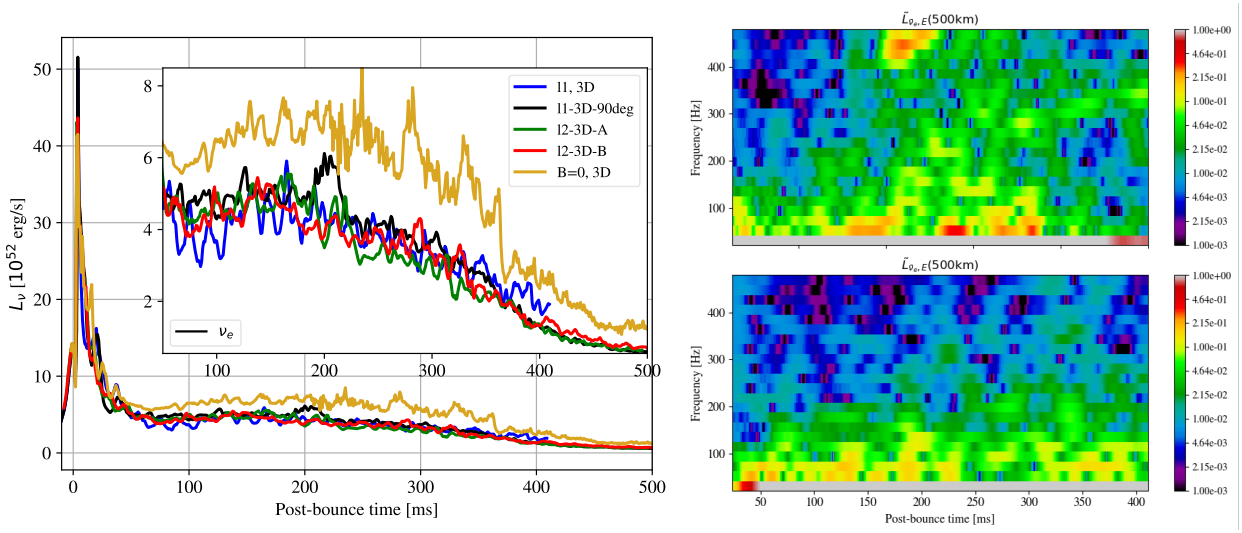

Fig. 4. Left: Non-axisymmetric density deviations on the equatorial plane during the development of the low $T/|W|$ instability. **Right:** Caption of the right panel.

5 Conclusions

We presented the current state-of-the-art in the numerical modeling of multi-messenger signals from CCSN, which will provide the fundamental tools to interpret the first multi-messenger observation of a nearby stellar explosion. Our analysis of recently published 3d MHD simulations with complex magnetic field structures (Bugli et al. 2021, 2022) sheds some light on the role that strong magnetic fields play in CCSN models with fast rotating progenitors. While in presence of strong rotation both the GW and neutrino signals are expected to display clear signatures of the dynamical low $T/|W|$ instability, in the case of magnetized CCSN such features are instead quenched due to the efficiency of the magnetic transport of angular momentum. In a forthcoming study, we will investigate more in detail the properties of co-rotational instabilities and their possible impact

on the dynamical amplification of magnetic fields, which will extend our current understanding of the PNS dynamics in the context of outstanding stellar explosions.

References

Andresen, H., Mller, B., Mller, E., & Janka, H.-T. 2017, Monthly Notices of the Royal Astronomical Society, 468, 2032

Bugli, M., Guilet, J., Foglizzo, T., & Obergaulinger, M. 2022, in prep.

Bugli, M., Guilet, J., & Obergaulinger, M. 2021, Monthly Notices of the Royal Astronomical Society, 507, 443, aDS Bibcode: 2021MNRAS.507..443B

Bugli, M., Guilet, J., Obergaulinger, M., Cerd-Durn, P., & Aloy, M. A. 2020, Monthly Notices of the Royal Astronomical Society, 492, 58

Burrows, A., Dessart, L., Livne, E., Ott, C. D., & Murphy, J. 2007, The Astrophysical Journal, 664, 416

Drout, M. R., Soderberg, A. M., Gal-Yam, A., et al. 2011, The Astrophysical Journal, 741, 97

Guilet, J., Reboul-Salze, A., Raynaud, R., Bugli, M., & Gallet, B. 2022, MRI-driven dynamo at very high magnetic Prandtl numbers, Tech. rep., publication Title: arXiv e-prints ADS Bibcode: 2022arXiv220508602G Type: article

Kawahara, H., Kuroda, T., Takiwaki, T., Hayama, K., & Kotake, K. 2018, The Astrophysical Journal, 867, 126, aDS Bibcode: 2018ApJ...867..126K

Kuroda, T., Arcones, A., Takiwaki, T., & Kotake, K. 2020, arXiv:2003.02004 [astro-ph], arXiv: 2003.02004

Murphy, J. W., Ott, C. D., & Burrows, A. 2009, The Astrophysical Journal, 707, 1173, aDS Bibcode: 2009ApJ...707.1173M

Nicholl, M., Smartt, S. J., Jerkstrand, A., et al. 2013, Nature, 502, 346

Obergaulinger, M. & á. Aloy, M. 2017, Monthly Notices of the Royal Astronomical Society: Letters, 469, L43

Obergaulinger, M. & Aloy, M. A. 2021, Monthly Notices of the Royal Astronomical Society, 503, 4942, aDS Bibcode: 2021MNRAS.503.4942O tex.ids= obergaulinger2020, obergaulinger2020b arXiv: 2008.07205

Ott, C. D. 2009, Classical and Quantum Gravity, 26, 063001

Passamonti, A. & Andersson, N. 2015, Monthly Notices of the Royal Astronomical Society, 446, 555

Raynaud, R., Cerd-Durn, P., & Guilet, J. 2021, arXiv e-prints, 2103, arXiv:2103.12445, arXiv: 2103.12445

Raynaud, R., Guilet, J., Janka, H.-T., & Gastine, T. 2020, Science Advances, 6, eaay2732

Reboul-Salze, A., Guilet, J., Raynaud, R., & Bugli, M. 2021, Astronomy and Astrophysics, 645, A109

Reboul-Salze, A., Guilet, J., Raynaud, R., & Bugli, M. 2022, MRI-driven $\alpha-\Omega$ dynamos in protoneutron stars, Tech. rep., publication Title: arXiv e-prints ADS Bibcode: 2021arXiv211102148R Type: article

Shibagaki, S., Kuroda, T., Kotake, K., & Takiwaki, T. 2020, Monthly Notices of the Royal Astronomical Society, 493, L138

Shibagaki, S., Kuroda, T., Kotake, K., & Takiwaki, T. 2021, Monthly Notices of the Royal Astronomical Society, 502, 3066, aDS Bibcode: 2021MNRAS.502.3066S

Shibata, M., Liu, Y. T., Shapiro, S. L., & Stephens, B. C. 2006, Physical Review D, 74, 104026, citation Key Alias: shibata2006b

Summa, A., Janka, H.-T., Melson, T., & Marek, A. 2018, The Astrophysical Journal, 852, 28

Takiwaki, T., Kotake, K., & Foglizzo, T. 2021, Monthly Notices of the Royal Astronomical Society, 508, 966, aDS Bibcode: 2021MNRAS.508..966T

Takiwaki, T., Kotake, K., & Sato, K. 2009, The Astrophysical Journal, 691, 1360

Takiwaki, T., Kotake, K., & Suwa, Y. 2016, Monthly Notices of the Royal Astronomical Society: Letters, 461, L112

Torres-Forn, A., Cerd-Durn, P., Obergaulinger, M., Muller, B., & Font, J. A. 2019, arXiv e-prints, arXiv:1902.10048

Woosley, S. E. & Heger, A. 2006, The Astrophysical Journal, 637, 914